



KEK preprint 2001-149
Belle preprint 2001-19

Determination of $|V_{cb}|$ using the semileptonic decay $\bar{B}^0 \rightarrow D^{*+}e^{-}\bar{\nu}$

Belle Collaboration

K. Abe⁹, K. Abe⁴³, R. Abe³², T. Abe⁴⁴, I. Adachi⁹, Byoung Sup Ahn¹⁷,
H. Aihara⁴⁵, M. Akatsu²⁵, Y. Asano⁵⁰, T. Aso⁴⁹, V. Aulchenko²,
T. Aushev¹⁴, A. M. Bakich⁴¹, Y. Ban³⁶, E. Banas³⁰, S. Behari⁹,
P. K. Behera⁵¹, A. Bondar², A. Bozek³⁰, T. E. Browder⁸, B. C. K. Casey⁸,
P. Chang²⁹, Y. Chao²⁹, B. G. Cheon⁴⁰, R. Chistov¹⁴, S.-K. Choi⁷, Y. Choi⁴⁰,
L. Y. Dong¹², A. Drutskoy¹⁴, S. Eidelman², V. Eiges¹⁴, C. W. Everton²³,
F. Fang⁸, H. Fujii⁹, C. Fukunaga⁴⁷, M. Fukushima¹¹, N. Gabyshev⁹,
A. Garmash^{2,9}, T. Gershon⁹, A. Gordon²³, R. Guo²⁷, J. Haba⁹,
H. Hamasaki⁹, K. Hanagaki³⁷, F. Handa⁴⁴, K. Hara³⁴, T. Hara³⁴,
N. C. Hastings²³, H. Hayashii²⁶, M. Hazumi⁹, E. M. Heenan²³, I. Higuchi⁴⁴,
T. Higuchi⁴⁵, T. Hojo³⁴, T. Hokuue²⁵, Y. Hoshi⁴³, K. Hoshina⁴⁸, S. R. Hou²⁹,
W.-S. Hou²⁹, S.-C. Hsu²⁹, H.-C. Huang²⁹, Y. Igarashi⁹, T. Iijima⁹, H. Ikeda⁹,
K. Inami²⁵, A. Ishikawa²⁵, H. Ishino⁴⁶, R. Itoh⁹, H. Iwasaki⁹, Y. Iwasaki⁹,
D. J. Jackson³⁴, P. Jalocha³⁰, H. K. Jang³⁹, J. H. Kang⁵⁴, J. S. Kang¹⁷,
P. Kapusta³⁰, N. Katayama⁹, H. Kawai³, H. Kawai⁴⁵, N. Kawamura¹,
T. Kawasaki³², H. Kichimi⁹, D. W. Kim⁴⁰, Heejong Kim⁵⁴, H. J. Kim⁵⁴,
H. O. Kim⁴⁰, Hyunwoo Kim¹⁷, S. K. Kim³⁹, T. H. Kim⁵⁴, K. Kinoshita⁵,
H. Konishi⁴⁸, S. Korpar^{22,15}, P. Krizan^{21,15}, P. Krokovny², R. Kulasiri⁵,
S. Kumar³⁵, A. Kuzmin², Y.-J. Kwon⁵⁴, J. S. Lange⁶, G. Leder¹³,
S. H. Lee³⁹, D. Liventsev¹⁴, R.-S. Lu²⁹, J. MacNaughton¹³, T. Matsubara⁴⁵,
S. Matsumoto⁴, T. Matsumoto²⁵, Y. Mikami⁴⁴, K. Miyabayashi²⁶,
H. Miyake³⁴, H. Miyata³², G. R. Moloney²³, S. Mori⁵⁰, T. Mori⁴,
A. Murakami³⁸, T. Nagamine⁴⁴, Y. Nagasaka¹⁰, Y. Nagashima³⁴,

T. Nakadaira⁴⁵, E. Nakano³³, M. Nakao⁹, J. W. Nam⁴⁰, Z. Natkaniec³⁰,
K. Neichi⁴³, S. Nishida¹⁸, O. Nitoh⁴⁸, S. Noguchi²⁶, T. Nozaki⁹, S. Ogawa⁴²,
T. Ohshima²⁵, T. Okabe²⁵, S. Okuno¹⁶, S. L. Olsen⁸, W. Ostrowicz³⁰,
H. Ozaki⁹, P. Pakhlov¹⁴, H. Palka³⁰, C. S. Park³⁹, C. W. Park¹⁷, H. Park¹⁹,
K. S. Park⁴⁰, L. S. Peak⁴¹, J.-P. Perroud²⁰, M. Peters⁸, L. E. Piiilonen⁵²,
E. Prebys³⁷, J. L. Rodriguez⁸, N. Root², M. Rozanska³⁰, J. Ryuko³⁴,
H. Sagawa⁹, Y. Sakai⁹, H. Sakamoto¹⁸, M. Satapathy⁵¹, A. Satpathy^{9,5},
S. Schrenk⁵, S. Semenov¹⁴, K. Senyo²⁵, M. E. Sevier²³, H. Shibuya⁴²,
B. Shwartz², J. B. Singh³⁵, S. Stanić⁵⁰, A. Sugiyama²⁵, K. Sumisawa⁹,
T. Sumiyoshi⁹, S. Suzuki⁵³, S. Y. Suzuki⁹, S. K. Swain⁸, T. Takahashi³³,
F. Takasaki⁹, M. Takita³⁴, K. Tamai⁹, N. Tamura³², J. Tanaka⁴⁵,
M. Tanaka⁹, Y. Tanaka²⁴, G. N. Taylor²³, Y. Teramoto³³, M. Tomoto⁹,
T. Tomura⁴⁵, S. N. Tovey²³, K. Trabelsi⁸, T. Tsuboyama⁹, T. Tsukamoto⁹,
S. Uehara⁹, K. Ueno²⁹, Y. Unno³, S. Uno⁹, Y. Ushiroda⁹, S. E. Vahsen³⁷,
K. E. Varvell⁴¹, C. C. Wang²⁹, C. H. Wang²⁸, J. G. Wang⁵², M.-Z. Wang²⁹,
Y. Watanabe⁴⁶, E. Won³⁹, B. D. Yabsley⁹, Y. Yamada⁹, M. Yamaga⁴⁴,
A. Yamaguchi⁴⁴, H. Yamamoto⁴⁴, Y. Yamashita³¹, M. Yamauchi⁹,
S. Yanaka⁴⁶, J. Yashima⁹, M. Yokoyama⁴⁵, K. Yoshida²⁵, Y. Yuan¹²,
Y. Yusa⁴⁴, C. C. Zhang¹², J. Zhang⁵⁰, H. W. Zhao⁹, Y. Zheng⁸, V. Zhilich²,
and D. Žontar⁵⁰

¹*Aomori University, Aomori*

²*Budker Institute of Nuclear Physics, Novosibirsk*

³*Chiba University, Chiba*

⁴*Chuo University, Tokyo*

⁵*University of Cincinnati, Cincinnati OH*

⁶*University of Frankfurt, Frankfurt*

⁷*Gyeongsang National University, Chinju*

⁸*University of Hawaii, Honolulu HI*

⁹*High Energy Accelerator Research Organization (KEK), Tsukuba*

¹⁰*Hiroshima Institute of Technology, Hiroshima*

¹¹*Institute for Cosmic Ray Research, University of Tokyo, Tokyo*

¹²*Institute of High Energy Physics, Chinese Academy of Sciences, Beijing*

¹³*Institute of High Energy Physics, Vienna*

¹⁴*Institute for Theoretical and Experimental Physics, Moscow*

¹⁵*J. Stefan Institute, Ljubljana*

¹⁶*Kanagawa University, Yokohama*

¹⁷*Korea University, Seoul*

¹⁸*Kyoto University, Kyoto*

¹⁹*Kyungpook National University, Taegu*

²⁰*IPHE, University of Lausanne, Lausanne*

- ²¹ *University of Ljubljana, Ljubljana*
²² *University of Maribor, Maribor*
²³ *University of Melbourne, Victoria*
²⁴ *Nagasaki Institute of Applied Science, Nagasaki*
²⁵ *Nagoya University, Nagoya*
²⁶ *Nara Women's University, Nara*
²⁷ *National Kaohsiung Normal University, Kaohsiung*
²⁸ *National Lien-Ho Institute of Technology, Miao Li*
²⁹ *National Taiwan University, Taipei*
³⁰ *H. Niewodniczanski Institute of Nuclear Physics, Krakow*
³¹ *Nihon Dental College, Niigata*
³² *Niigata University, Niigata*
³³ *Osaka City University, Osaka*
³⁴ *Osaka University, Osaka*
³⁵ *Panjab University, Chandigarh*
³⁶ *Peking University, Beijing*
³⁷ *Princeton University, Princeton NJ*
³⁸ *Saga University, Saga*
³⁹ *Seoul National University, Seoul*
⁴⁰ *Sungkyunkwan University, Suwon*
⁴¹ *University of Sydney, Sydney NSW*
⁴² *Toho University, Funabashi*
⁴³ *Tohoku Gakuin University, Tagajo*
⁴⁴ *Tohoku University, Sendai*
⁴⁵ *University of Tokyo, Tokyo*
⁴⁶ *Tokyo Institute of Technology, Tokyo*
⁴⁷ *Tokyo Metropolitan University, Tokyo*
⁴⁸ *Tokyo University of Agriculture and Technology, Tokyo*
⁴⁹ *Toyama National College of Maritime Technology, Toyama*
⁵⁰ *University of Tsukuba, Tsukuba*
⁵¹ *Utkal University, Bhubaneswer*
⁵² *Virginia Polytechnic Institute and State University, Blacksburg VA*
⁵³ *Yokkaichi University, Yokkaichi*
⁵⁴ *Yonsei University, Seoul*

Abstract

We present a measurement of the Cabibbo-Kobayashi-Maskawa (CKM) matrix element $|V_{cb}|$ using a 10.2 fb^{-1} data sample recorded at the $\Upsilon(4S)$ resonance with the Belle detector at the KEKB asymmetric e^+e^- storage ring. By extrapolating the differential decay width of the $\bar{B}^0 \rightarrow D^{*+}e^-\bar{\nu}$ decay to the kinematic limit at which the D^{*+} is at rest with respect to the \bar{B}^0 , we extract the product of $|V_{cb}|$ with the normalization of the decay form factor $F(1)$, $|V_{cb}| F(1) = (3.54 \pm 0.19 \pm 0.18) \times 10^{-2}$, where the first error is statistical and the second is systematic. A value of $|V_{cb}| =$

$(3.88 \pm 0.21 \pm 0.20 \pm 0.19) \times 10^{-2}$ is obtained using a theoretical calculation of $F(1)$, where the third error is due to the theoretical uncertainty in the value of $F(1)$. The branching fraction $\mathcal{B}(\bar{B}^0 \rightarrow D^{*+} e^- \bar{\nu})$ is measured to be $(4.59 \pm 0.23 \pm 0.40) \times 10^{-2}$.

PACS: 12.15.Hh, 13.30.Ce, 13.20.Hw

1 Introduction

Accurate measurements of CKM matrix elements are important to constrain the Standard Model. Knowledge of $|V_{cb}|$ is needed to relate a number of experimentally measured CP violating observables to the Wolfenstein parameters [1] through which they are usually illustrated. $|V_{cb}|$ can be determined by studying exclusive $\bar{B}^0 \rightarrow D^{*+} \ell^- \bar{\nu}$ decays using Heavy Quark Effective Theory (HQET) [2], an exact theory in the limit of infinite quark masses. The development of HQET yields an expression for the $\bar{B}^0 \rightarrow D^{*+} \ell^- \bar{\nu}$ decay rate in terms of a single unknown form factor. The form factor is parameterized in terms of y , the inner product of the \bar{B}^0 and D^{*+} four-velocities:

$$y = v_{\bar{B}^0} \cdot v_{D^{*+}} = \frac{M_{\bar{B}^0}^2 + M_{D^{*+}}^2 - q^2}{2M_{\bar{B}^0} M_{D^{*+}}},$$

where $M_{\bar{B}^0}$ and $M_{D^{*+}}$ are masses of the \bar{B}^0 and D^{*+} meson respectively and $q^2 = (p_{\bar{B}^0} - p_{D^{*+}})^2$. Here, and in what follows, p stands for the four-momentum vector of the particle in subscript.

The form factor $F(y)$ is expressed as the product of a normalization factor $F(1)$ and a shape function which is constrained by a dispersion relation [3]. We extract the product of $|V_{cb}|$ and $F(1)$ from extrapolation of the data to the zero-recoil point $y = 1$, where the D^{*+} is at rest with respect to the \bar{B}^0 .

At this kinematic point, HQET allows us to calculate $F(1)$ with small and controllable theoretical errors. There are several corrections to the heavy quark limit $F(1) = 1$ as follows:

$$F(1) = \eta_{\text{QED}} \eta_A (1 + \delta_{1/m^2} + \dots).$$

QED correction factors up to leading logarithmic order provide $\eta_{\text{QED}} \approx 1.007$ [4]. η_A is a short-distance correction arising from the finite QCD renormalization of the flavor-changing axial current at the point of zero recoil. The first order term in the non-perturbative expansion in powers of $1/m_Q$ vanishes by virtue of Luke's theorem [5], and δ_{1/m^2} represents the second order correction. By contrast, the form factor of $\bar{B} \rightarrow D \ell \bar{\nu}$ decay is not protected against $1/m_Q$ corrections at zero recoil [6], hence the comparison of results from $\bar{B} \rightarrow D^* \ell \bar{\nu}$ with $\bar{B} \rightarrow D \ell \bar{\nu}$ [7]-[9] provides some measure of the size of corrections to HQET. Results for η_{QED} and η_A are combined with their errors added linearly to give $F(1) = 0.913 \pm 0.042$ [10]. This value of $F(1)$ is in good agreement with the latest lattice QCD calculation, $F(1) = 0.9130_{-0.0348}^{+0.0293}$ [11].

This method currently gives the smallest theoretical error in the extraction of $|V_{cb}|$. Measurements of $|V_{cb}|$ based on the dispersion relation have been

published by the OPAL [12] and DELPHI [13] collaborations using B mesons produced in Z^0 decays at LEP and reported by the CLEO collaboration [14] operating at the $\Upsilon(4S)$ resonance.

In this paper, we present a measurement of the branching fraction of the exclusive semileptonic B decay $\bar{B}^0 \rightarrow D^{*+}e^-\bar{\nu}$, and a determination of $|V_{cb}|$. The charge conjugate mode is implicitly included. For this precise measurement we use $\bar{B}^0 \rightarrow D^{*+}e^-\bar{\nu}$ and not $\bar{B}^0 \rightarrow D^{*+}\mu^-\bar{\nu}$ since the electron identification efficiency plateau has a wider range in both momentum and polar angle than that of muons, leading to a better control of systematic uncertainties.

The data correspond to an integrated luminosity of 10.2 fb^{-1} accumulated at the $\Upsilon(4S)$ resonance with the Belle detector [15] at KEKB [16], an asymmetric e^+e^- storage ring. This corresponds to $10.8 \times 10^6 B\bar{B}$ events. An additional sample with an integrated luminosity of 0.6 fb^{-1} taken at an energy 60 MeV below the $\Upsilon(4S)$ resonance is used as a control sample to check continuum processes. A GEANT [17] based Monte Carlo (MC) simulation is used to study the signal decay mode and also to estimate some backgrounds.

2 Belle Detector

Belle is a general-purpose detector which includes a 1.5 T superconducting solenoid magnet. Charged particle tracking is provided by a silicon vertex detector (SVD) and a central drift chamber (CDC) that surround the interaction region. The SVD consists of three layers of double-sided silicon strip detectors; one side of each detector measures the z coordinate and the other the $r - \phi$ coordinate. The CDC has 50 cylindrical layers of anode wires; the inner three layers have instrumented cathodes for z coordinate measurements. The charged particle acceptance covers laboratory polar angles between $\theta = 17^\circ$ and 150° corresponding to about 92% of the full solid angle in the center of mass (CM) frame. The momentum resolution is $(\sigma_{|\mathbf{p}_t|}/|\mathbf{p}_t|)^2 = (0.0019|\mathbf{p}_t|)^2 + (0.0030)^2$, where \mathbf{p}_t is the transverse momentum in the laboratory frame, in units of GeV/c .

Charged hadron identification is provided by dE/dx measurements in the CDC, a mosaic of 1188 aerogel Čerenkov counters (ACC), and a barrel-like array of 128 time-of-flight scintillation counters (TOF). The dE/dx measurements have a resolution for hadron tracks of 6.9% and are useful for π/K separation for $|\mathbf{p}_{\text{lab}}| < 0.8 \text{ GeV}/c$ and $|\mathbf{p}_{\text{lab}}| > 2.5 \text{ GeV}/c$. Here, and in what follows, \mathbf{p}_{lab} is the three-momentum vector in the laboratory frame and \mathbf{p} denotes the three-momentum vector in the CM frame. The TOF system has a time resolution for hadrons of $\sigma \simeq 100 \text{ ps}$ and provides π/K separation for $|\mathbf{p}_{\text{lab}}| < 1.2 \text{ GeV}/c$. The ACC covers the range $1.2 \text{ GeV}/c < |\mathbf{p}_{\text{lab}}| <$

3.5 GeV/ c and the refractive indices of the ACC elements vary with polar angle to match the kinematics of the asymmetric energy environment of Belle. Particle identification probabilities are determined from the combined response of the three systems.

The electromagnetic calorimeter (ECL) consists of an array of 8736 CsI(Tl) crystals located in the magnetic volume covering the same solid angle as the charged particle tracking system. The energy resolution for electromagnetic showers is $(\sigma_E/E)^2 = (0.013)^2 + (0.0007/E)^2 + (0.008/E^{1/4})^2$, where E is in GeV.

Electron identification is based on a combination of dE/dx measurements in the CDC, the response of the ACC, and the position, shape and the ratio of the total cluster energy registered in the ECL and particle momentum. The electron identification efficiency, determined by embedding simulated tracks in multihadron data, is greater than 92% for tracks reconstructed in the CDC with $|\mathbf{p}_{\text{lab}}| > 1.0$ GeV/ c . The hadron misidentification probability, determined using $K_S^0 \rightarrow \pi^+\pi^-$ decays, is below 0.3%.

The 1.5 T magnetic field is returned via an iron yoke that is instrumented to detect muons and K_L mesons (KLM). The KLM covers polar angles between $\theta = 20^\circ$ and 155° and the overall muon identification efficiency, determined by a track embedding study similar to that used for the electron case, is greater than 87% for tracks reconstructed in the CDC with $|\mathbf{p}_{\text{lab}}| > 1$ GeV/ c . The corresponding pion misidentification probability determined from $K_S^0 \rightarrow \pi^+\pi^-$ decays is less than 2%.

3 Event Reconstruction

We reconstruct $\bar{B}^0 \rightarrow D^{*+}e^-\bar{\nu}$ decays using the decay chain $D^{*+} \rightarrow D^0\pi^+$, $D^0 \rightarrow K^-\pi^+$ and requiring the electron to be cleanly identified. In order to suppress the jet-like $e^+e^- \rightarrow q\bar{q}$ continuum background, the ratio of the second to zeroth Fox-Wolfram moments [18] is required to be less than 0.4. This requirement removes 43% of the continuum background whilst it retains 93% of the $\bar{B}^0 \rightarrow D^{*+}e^-\bar{\nu}$ signal. Each event is required to contain at least one electron candidate with momentum in the CM frame in the range 1.00 GeV/ c to 2.45 GeV/ c .

After a $K^-\pi^+$ combination is selected, a D^0 decay vertex is reconstructed. D^0 candidates are required to satisfy track quality cuts based on their impact parameters relative to the $K^-\pi^+$ vertex: $\Delta r < 0.2$ cm and $\Delta z < 0.5$ cm. The $D^0 \rightarrow K^-\pi^+$ candidates must have an invariant mass within 3σ of the nominal D^0 value, where $\sigma \simeq 6$ MeV/ c^2 .

We combine D^0 candidates with slow pion candidates (π_s^+) to fully reconstruct D^{*+} mesons in the mode $D^{*+} \rightarrow D^0\pi^+$. The mass difference ($\Delta M = M_{K^-\pi^+\pi_s^+} - M_{K^-\pi^+}$) is required to lie within 3 MeV/ c^2 of the nominal peak position (Figure 1). Furthermore the momentum of D^{*+} candidates must satisfy $|\mathbf{p}_{D^{*+}}| < 0.5\sqrt{E_{\text{beam}}^2 - M_{D^{*+}}^2}$ to be consistent with a B decay hypothesis, where E_{beam} is the beam energy. This requirement retains nearly 100% of signal events whilst it rejects 34% of the continuum background. A $D^0 - e^-$ vertex is constructed and the electron momentum vector is recomputed with the vertex constraint.

Since the only missing particle in the $\bar{B}^0 \rightarrow D^{*+}e^-\bar{\nu}$ decay is the neutrino, we expect the square of the missing four-momentum to vanish, $p_{\text{miss}}^2 \equiv p_{\bar{\nu}}^2 = (p_{\bar{B}^0} - p_{D^{*+}e^-})^2 = 0$, where $p_{D^{*+}e^-} = p_{D^{*+}} + p_{e^-}$. This can be expressed in the CM frame:

$$p_{\text{miss}}^2 = M_{\bar{B}^0}^2 + M_{D^{*+}e^-}^2 - 2E_{\bar{B}^0}E_{D^{*+}e^-} + 2|\mathbf{p}_{\bar{B}^0}||\mathbf{p}_{D^{*+}e^-}|\cos\theta_{\bar{B}^0,D^{*+}e^-},$$

where $E_{\bar{B}^0}$ is replaced by E_{beam} from which $|\mathbf{p}_{\bar{B}^0}|$ is calculated. Neglecting the last term since $|\mathbf{p}_{\bar{B}^0}|$ is small in the CM frame (~ 340 MeV/ c), we define the square of missing mass as follows:

$$M_{\text{miss}}^2 = M_{\bar{B}^0}^2 + M_{D^{*+}e^-}^2 - 2E_{\bar{B}^0}E_{D^{*+}e^-}.$$

We make the cut $M_{\text{miss}}^2 < 1$ GeV $^2/c^4$ to suppress the background from $\bar{B}^0 \rightarrow D^{**}e^-\bar{\nu}$, which has an additional pion (by D^{**} , we denote the sum of resonant and non-resonant states). The efficiency of the cut on M_{miss}^2 is about 96% for $\bar{B}^0 \rightarrow D^{*+}e^-\bar{\nu}$ and 53% for $\bar{B}^0 \rightarrow D^{**}e^-\bar{\nu}$. Using the condition $p_{\text{miss}}^2 = 0$, we can extract $\cos\theta_{\bar{B}^0,D^{*+}e^-}$ as follows:

$$\cos\theta_{\bar{B}^0,D^{*+}e^-} = \frac{2E_{\bar{B}^0}E_{D^{*+}e^-} - M_{\bar{B}^0}^2 - M_{D^{*+}e^-}^2}{2|\mathbf{p}_{\bar{B}^0}||\mathbf{p}_{D^{*+}e^-}|}.$$

The quantity $\cos\theta_{\bar{B}^0,D^{*+}e^-}$ is highly correlated with the estimated value of M_{miss}^2 but allows us to impose a kinematic consistency condition through the requirement $|\cos\theta_{\bar{B}^0,D^{*+}e^-}| < 1$. This requirement removes 66% of the $\bar{B}^0 \rightarrow D^{**}e^-\bar{\nu}$ background and 81% of the continuum background whilst keeping 88% of the signal.

The reconstructed \bar{B}^0 mass $M_{\bar{B}^0}^{\text{rec}}$ is defined as

$$M_{\bar{B}^0}^{\text{rec}} = \sqrt{E_{\text{beam}}^2 - |\mathbf{p}_{D^{*+}} + \mathbf{p}_{e^-} + \mathbf{p}_{\bar{\nu}}|^2},$$

where the neutrino momentum is calculated using all the reconstructed tracks

and clusters in the event: $\mathbf{p}_{\bar{\nu}} = -\sum_i \mathbf{p}_i$. In this analysis, we use this information only to make a loose consistency requirement of $M_{\bar{B}^0}^{\text{rec}} > 5.0 \text{ GeV}/c^2$. This cut value gives 95% efficiency for the signal mode; it removes 18% of continuum background.

Since this analysis is not based on a full reconstruction of the \bar{B}^0 , we do not calculate q^2 using missing momentum information. Instead, we compute y by taking the average of the values obtained with the two extreme configurations of the \bar{B}^0 and D^{*+} directions consistent with $\mathbf{p}_{D^{*+}}$, \mathbf{p}_{e^-} and the value of $\cos\theta_{\bar{B}^0, D^{*+}e^-}$ calculated above. We reject the unphysical region in the distribution of \tilde{y} , which denotes the measured y value. The resolution of y has been studied using MC, and is found to be accurately modeled by a symmetric Gaussian with $\sigma \simeq 0.04$.

The overall signal reconstruction efficiency is 6.0% after all event selection criteria.

4 Background Subtraction

The background sources fall into five categories: combinatorial, correlated, uncorrelated, fake electron and continuum. The largest source is the combinatorial background in the D^{*+} reconstruction. The level of this background is determined from a fit to the ΔM distribution, using a phase space shape for the background. The corresponding shape of the background in the variable \tilde{y} is deduced from events in a sideband region, which is defined as $0.155 \text{ GeV}/c^2 < \Delta M < 0.165 \text{ GeV}/c^2$ as shown in Figure 1.

The contributions from other sources of background are estimated using MC. Correlated background occurs when a \bar{B}^0 meson decays to a final state containing a D^{*+} and an e^- through channels other than $\bar{B}^0 \rightarrow D^{*+}e^-\bar{\nu}$. The largest source is due to the process $\bar{B}^0 \rightarrow D^{**}e^-\bar{\nu}$. From a simulation based on the ISGW2 [19], and Goity and Roberts models [20], we find this background accounts for about 9% of the raw yield. Hence this is a large source of background.

In uncorrelated background events, the D^* originates from the decay of the \bar{B} and the electron originates from the partner B . The electrons in this background must come from secondary B meson decay products or $B^0 - \bar{B}^0$ mixing in order to have the correct charge. It is also possible to have electrons from the decay or misidentification of light hadrons and these are classified as fake electron background. The fake electron background is estimated using MC without primary electrons from \bar{B} decays. A very small contribution to the signal yield is found. The size of the continuum background is measured using

$q\bar{q}$ MC.

In Figure 2, the raw yield and various backgrounds are displayed as a function of \tilde{y} and electron momentum in the CM frame. Table 1 shows the expected background contributions to the raw yield.

5 Form Factor Parameterization

The differential rate for the $\bar{B}^0 \rightarrow D^{*+}e^{-}\bar{\nu}$ decay is given by [21]

$$\frac{d\Gamma}{dy} = \frac{G_F^2}{48\pi^3} M_{D^{*+}}^3 (M_{\bar{B}^0} - M_{D^{*+}})^2 g(y) |V_{cb}|^2 F(y)^2,$$

$$g(y) = \sqrt{y^2 - 1} (y + 1)^2 \left[1 + 4 \frac{y}{y + 1} \frac{1 - 2yr + r^2}{(1 - r)^2} \right],$$

where G_F is the Fermi coupling constant and $r = M_{D^{*+}}/M_{\bar{B}^0}$. We approximate $F(y)$ with a Taylor series expansion around $y = 1$:

$$F(y) = F(1)[1 - \rho_F^2(y - 1) + c(y - 1)^2 + \mathcal{O}(y - 1)^3].$$

Early $|V_{cb}|$ measurements [22]-[25] used this expansion neglecting the second order term (this is called the linear form factor parameterization). However, since a determination of $|V_{cb}|$ requires the extrapolation of the differential decay rate to $y = 1$, constraints on the shape of the form factor are highly desirable to reduce the uncertainties associated with this extrapolation. A suitable framework to derive such constraints on heavy meson form factors has recently been provided by dispersion relations [26]-[30].

To use the relevant dispersion relation [3] we relate $F(y)$ to the axial vector form factor $h_{A_1}(y)$ using [2,31]

$$g(y)F(y)^2 = \sqrt{y^2 - 1} (y + 1)^2 h_{A_1}(y)^2$$

$$\times \left\{ 2 \left[\frac{1 - 2yr + r^2}{(1 - r)^2} \right] (1 + R_1(y))^2 \frac{y - 1}{y + 1} + \left[1 + (1 - R_2(y)) \frac{y - 1}{1 - r} \right]^2 \right\}.$$

$R_1(y)$ and $R_2(y)$ are given by:

$$R_1(y) \approx R_1(1) - 0.12(y - 1) + 0.05(y - 1)^2,$$

$$R_2(y) \approx R_2(1) + 0.11(y - 1) - 0.06(y - 1)^2.$$

Using the results of the dispersion relation, $h_{A_1}(y)/h_{A_1}(1)$ depends only on a single unknown parameter $\rho_{A_1}^2$:

$$\frac{h_{A_1}(y)}{h_{A_1}(1)} \approx 1 - 8\rho_{A_1}^2 z + (53\rho_{A_1}^2 - 15)z^2 - (231\rho_{A_1}^2 - 91)z^3,$$

where $z = (\sqrt{y+1} - \sqrt{2})/(\sqrt{y+1} + \sqrt{2})$. It can be seen that $h_{A_1}(y) \rightarrow F(y)$ in the limit $y \rightarrow 1$, hence $h_{A_1}(1) = F(1)$. Our main analysis uses this dispersion relation parameterization. The dispersive bound used in this analysis requires that $-0.14 < \rho_{A_1}^2 < 1.54$ [3].

6 Fit and Results

After subtraction of background, we fit the final yield as a function of y for $|V_{cb}|F(1)$ and $\rho_{A_1}^2$. We use $R_1(1) = 1.3 \pm 0.1$ and $R_2(1) = 0.8 \pm 0.2$ which are obtained using HQET and QCD sum rules [2]. We minimize the following variable:

$$\chi^2 = \sum_{i=1}^{N_{\text{bin}}=10} \left(\frac{N_i^{\text{obs}} - \sum_{j=1}^{N_{\text{bin}}} \epsilon_{ij} N_j}{\sigma_{N_i^{\text{obs}}}} \right)^2,$$

where N_{bin} is the number of bins over the range $1.000 < \tilde{y} < 1.504$, N_i^{obs} is the yield in the i th \tilde{y} bin, $\sigma_{N_i^{\text{obs}}}$ is the statistical error of N_i^{obs} and N_j is the number of decays in the j th bin, given by

$$N_j = 2N_{B\bar{B}} f_{00} \tau_{\bar{B}^0} \mathcal{B}(D^{*+} \rightarrow D^0 \pi^+) \mathcal{B}(D^0 \rightarrow K^- \pi^+) \int_{y_j} \frac{d\Gamma}{dy} dy,$$

where the integral is over the range of y in the j th bin, $N_{B\bar{B}}$ is the number of $B\bar{B}$ pairs in the sample and f_{00} is the $\Upsilon(4S) \rightarrow B^0 \bar{B}^0$ branching fraction and is taken to be 0.5; $\tau_{\bar{B}^0}$ is the \bar{B}^0 lifetime, $\mathcal{B}(D^{*+} \rightarrow D^0 \pi^+)$ is the $D^{*+} \rightarrow D^0 \pi^+$ branching fraction, $\mathcal{B}(D^0 \rightarrow K^- \pi^+)$ is the $D^0 \rightarrow K^- \pi^+$ branching fraction and these values are taken from [32]. The efficiency matrix element ϵ_{ij} gives the probability that events generated in bin j in y are reconstructed in bin i . Typical values of the diagonal elements are in the range 0.023–0.033, while the elements for neighboring bins are in the range 0.007–0.021. A result of

$$\begin{aligned} |V_{cb}| F(1) &= (3.54 \pm 0.19) \times 10^{-2}, \\ \rho_{A_1}^2 &= 1.35 \pm 0.17 \end{aligned}$$

is obtained, where the errors are statistical only. The correlation coefficient between $|V_{cb}|F(1)$ and $\rho_{A_1}^2$ is 0.91 and the χ^2 of the fit is 3.38 for 8 degrees of freedom. The fit results are shown in Figure 3. By summation of the N_j obtained above over all bins, the branching fraction of $\mathcal{B}(\bar{B}^0 \rightarrow D^{*+}e^-\bar{\nu})$ is determined to be

$$\mathcal{B}(\bar{B}^0 \rightarrow D^{*+}e^-\bar{\nu}) = (4.59 \pm 0.23) \times 10^{-2},$$

where again the error is statistical only.

We have studied the impact of precise values of the $R_1(1)$ and $R_2(1)$ coefficients on the results of our analysis by using the CLEO measurement, $R_1(1) = 1.18 \pm 0.32$ and $R_2(1) = 0.71 \pm 0.23$ [33]. In addition, we have studied the case of the linear form factor defined above. This is a common approximation in the limit of heavy quark symmetry, in which $R_1(y) = R_2(y) = 1$ [2]. In Table 2 the results of the three different fits are compared.

In order to deal with the smearing effects due to the experimental resolution, an unfolding method is applied [34]. The unfolded data of $|V_{cb}|F(y)$ as a function of y is shown in Figure 4.

7 Systematic Errors

The systematic uncertainties in the result from each possible source are estimated by changing the input values in the $|V_{cb}|$ fitting procedure. A summary of the contributions to the systematic errors is given in Table 3.

The systematic uncertainty in the number of $B\bar{B}$ events is estimated by varying $N_{B\bar{B}}$ within its measured uncertainty. The various fit inputs, the \bar{B}^0 lifetime and D^{*+}, D^0 branching fractions, are varied according to the errors given in [32]. Since the calculation of the branching fraction in [32] is based on the assumption of equal B^+B^- and $B^0\bar{B}^0$ production, we do not take into account the uncertainty of f_{00} .

The uncertainty in the tracking efficiency for high momentum tracks is determined using $\eta \rightarrow \pi^+\pi^-\pi^0$ and $\eta \rightarrow \gamma\gamma$ decays. By comparing the numbers of reconstructed η 's between data and MC, we obtain an error of 2.5% on $|V_{cb}|F(1)$.

The efficiency for identifying electrons is evaluated by embedding single simulated electrons into hadronic events as well as $J/\psi \rightarrow e^+e^-$ events. We find that the uncertainty in the electron identification efficiency leads to a 1.0% systematic error on $|V_{cb}|F(1)$.

For D^0 reconstruction, three efficiencies are combined: kaon identification, pion identification and vertexing efficiencies. The particle identification efficiencies are obtained from data using the fact that the slow pion from D^{*+} decay allows the decay, $D^{*+} \rightarrow D^0\pi^+$, followed by $D^0 \rightarrow K^-\pi^+$, to be reconstructed without relying on particle identification. The systematic error in D^0 reconstruction is calculated from the measurement error (2.2%) of the efficiency in data. We find a systematic error of 1.4% on $|V_{cb}| F(1)$.

The slow pion reconstruction is mainly affected by the event environment and by material in the detectors. The former effect is evaluated by the track embedding method. It results in an uncertainty of 3.4%. The latter effect is estimated to be 3.7% by varying the energy loss in the inner detectors in the MC simulation. In total we find an uncertainty of 5.0% in the slow pion efficiency, leading to 2.6% uncertainty in $|V_{cb}| F(1)$.

The fit of $|V_{cb}| F(1)$ depends on the resolution of y , which is a function of the \bar{B}^0 and D^{*+} four-momentum vectors and of the beam energy. Therefore we change the \bar{B}^0 mass, D^{*+} mass and the beam energy by their uncertainties to estimate the contribution from these sources. We find a 1.1% change in $|V_{cb}| F(1)$.

We estimate the uncertainty from the combinatorial background subtraction by changing the sideband region and the fitting function, and assign a systematic error of 1.0% on $|V_{cb}| F(1)$.

By varying the branching fractions of the contributing modes in MC, the systematic error due to correlated background is determined to be 1.4%. We also estimate the size of the $\bar{B}^0 \rightarrow D^{*+}e^-\bar{\nu}$ background from data by fitting the M_{miss}^2 distribution. In this fit, the normalizations of the other background components are fixed and the shapes of the $D^{*+}e^-\bar{\nu}$ and $D^{**}e^-\bar{\nu}$ events come from MC. Using this method, we find 72 ± 8 background events, which is compatible with the number derived from MC within the systematic error.

The fraction of uncorrelated background in MC is varied by 100%, leading to a systematic error of 0.4% on $|V_{cb}| F(1)$. The uncertainty due to the fake electron background is estimated by varying the misidentification rate in MC according to the measured electron misidentification rate $0.20 \pm 0.02\%$ determined from $K_S^0 \rightarrow \pi^+\pi^-$ decays. The continuum background may be miscalculated if the $q\bar{q}$ background is inaccurately modeled in MC. The size of the continuum background is varied by 50%, giving 0.5% uncertainty on $|V_{cb}| F(1)$. We also check this background using the 0.6 fb^{-1} off-resonance data sample; the result is compatible with the MC estimate.

The uncertainty related to the finite MC statistics used to measure the efficiency matrix is measured by including the errors of the matrix elements in the fit. We denote this effect, 1.7% on $|V_{cb}| F(1)$, as MC statistics.

The $R_1(1)$ and $R_2(1)$ are related to the electron momentum distribution. To estimate this effect, we vary $R_1(1)$ and $R_2(1)$ within the errors given by [2] and find a resultant 11.8% uncertainty on $\rho_{A_1}^2$.

To test the stability of the result, several systematic checks were made. The requirements on the second Fox-Wolfram moment, the $K^-\pi^+$ invariant mass and the square of the missing mass were individually tightened; in each case no discrepancy was found. The analysis was also performed for a narrower range of electron momentum; again a consistent result was found.

8 Conclusion

In conclusion, we have measured the y distribution of $\bar{B}^0 \rightarrow D^{*+}e^-\bar{\nu}$ decays to obtain $|V_{cb}|F(1)$ and the slope of the form factor using a dispersion relation. The results are

$$|V_{cb}|F(1) = (3.54 \pm 0.19 \pm 0.18) \times 10^{-2},$$

$$\rho_{A_1}^2 = 1.35 \pm 0.17 \pm 0.19,$$

with a correlation coefficient between $|V_{cb}|F(1)$ and $\rho_{A_1}^2$ of 0.91. From the same fit, we extract the branching fraction

$$\mathcal{B}(\bar{B}^0 \rightarrow D^{*+}e^-\bar{\nu}) = (4.59 \pm 0.23 \pm 0.40) \times 10^{-2}.$$

These results are consistent with other published measurements from CESR [23] and LEP [12,13].

Using $F(1) = 0.913 \pm 0.042$ [10], the following value of $|V_{cb}|$ is obtained:

$$|V_{cb}| = (3.88 \pm 0.21 \pm 0.20 \pm 0.19) \times 10^{-2},$$

where the first error is statistical, the second is systematic and the third is theoretical.

Acknowledgments

We wish to thank the KEKB accelerator group for the excellent operation of the KEKB accelerator. We acknowledge support from the Ministry of Education, Culture, Sports, Science, and Technology of Japan and the Japan Society for the Promotion of Science; the Australian Research Council and

the Australian Department of Industry, Science and Resources; the Department of Science and Technology of India; the BK21 program of the Ministry of Education of Korea and the Center for High Energy Physics sponsored by the KOSEF; the Polish State Committee for Scientific Research under contract No.2P03B 17017; the Ministry of Science and Technology of Russian Federation; the National Science Council and the Ministry of Education of Taiwan; and the U.S. Department of Energy.

References

- [1] L. Wolfenstein, Phys. Rev. Lett. **51**, 1945 (1983).
- [2] M. Neubert, Phys. Rep. **245**, 259 (1994).
- [3] I. Caprini, L. Lellouch, M. Neubert, Nucl. Phys. B **530**, 153 (1998).
- [4] A. Sirlin, Nucl. Phys. B **196**, 83 (1982).
- [5] M. Luke, Phys. Lett. B **252**, 447 (1990).
- [6] M. Neubert and V. Rieckert, Nucl. Phys. B **382**, 97 (1992).
- [7] D. Buskulic *et al.* [ALEPH Collaboration], Phys. Lett. B **395**, 373 (1997).
- [8] J. Bartelt *et al.* [CLEO Collaboration], Phys. Rev. Lett. **82**, 3746 (1999).
- [9] K. Abe *et al.* [Belle Collaboration], hep-ex/0111082, submitted to Phys. Lett. B.
- [10] M. Neubert in BaBar Physics Book, P. F. Harrison and H. R. Quinn (editors), SLAC-R-504 (1998).
- [11] S. Hashimoto *et al.*, hep-ph/0110253, FERMILAB-PUB-01/317-T (2001).
- [12] G. Abbiendi *et al.* [OPAL Collaboration], Phys. Lett. B **842**, 15 (2000).
- [13] P. Abreu *et al.* [DELPHI Collaboration], Phys. Lett. B **510**, 55 (2001).
- [14] J. P. Alexander *et al.* [CLEO Collaboration], hep-ex/0007052, CLEO-CONF-00-03 (2000).
- [15] K. Abe *et al.* [Belle Collaboration], KEK Progress Report 2000-4 (2000), to be published in Nucl. Inst. and Meth. A.
- [16] KEKB B Factory Design Report, KEK Report 95-7 (1995), unpublished; Y. Funakoshi *et al.*, Proc. 2000 European Particle Accelerator Conference, Vienna (2000).
- [17] R. Brun *et al.*, GEANT 3.21, CERN Report No. DD/EE/84-1 (1987).
- [18] G. Fox and S. Wolfram, Phys. Rev. Lett **41**, 1581 (1978).

- [19] N. Isgur and D. Scora, Phys. Rev. D **52**, 2783 (1995); N. Isgur, D. Scora, B. Grinstein, and M. B. Wise, Phys. Rev. D **39**, 799 (1989).
- [20] J. L. Goity and W. Roberts, Phys. Rev. D **51**, 3459 (1995).
- [21] N. Neubert, Phys. Lett. B **264**, 455 (1991); B **338**, 84 (1994).
- [22] H. Albrecht *et al.* [ARGUS Collaboration], Z. Phys. C **57**, 533 (1993).
- [23] B. Barish *et al.* [CLEO Collaboration], Phys. Rev. D **51**, 1014 (1995).
- [24] D. Buskulic *et al.* [ALEPH Collaboration], Phys. Lett. B **359**, 373 (1995).
- [25] P. Abreu *et al.* [DELPHI Collaboration], Z. Phys. C **71**, 539 (1996).
- [26] E. de Rafael and J. Taron, Phys. Lett. B **282**, 215 (1992).
- [27] I. Caprini, Z. Phys. C **61**, 651 (1994).
- [28] C. G. Boyd, B. Grinstein and R. F. Lebed, Phys. Lett. B **353**, 306 (1995); Nucl. Phys. B **461**, 493 (1996).
- [29] I. Caprini and M. Neubert, Phys. Lett. B **380**, 376, (1996).
- [30] C. G. Boyd, B. Grinstein and R. F. Lebed, Phys. Rev. D **56**, 6895 (1997).
- [31] Int. J. Mod. Phys. A **11**, 4173 (1996).
- [32] D. E. Groom *et al.* [Particle Data Group Collaboration], Eur. Phys. J. C **15**, 1 (2000).
- [33] J. E. Duboscq *et al.* [CLEO Collaboration], Phys. Rev. Lett. **76**, 3898 (1996).
- [34] G. D'Agostini, Nucl. Inst. and Meth. A **362**, 487 (1995).

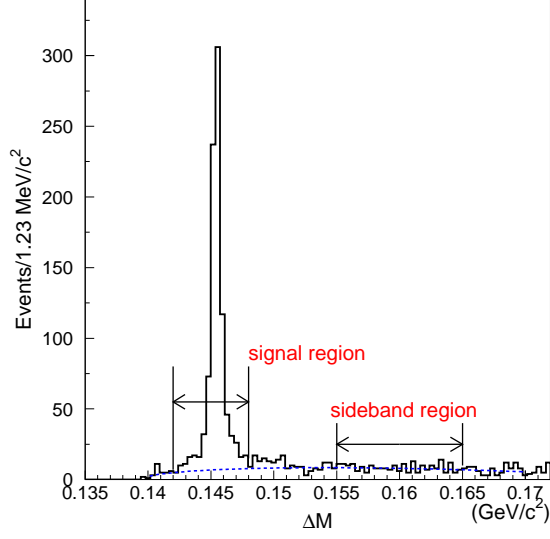


Fig. 1. ΔM distribution for $\bar{B}^0 \rightarrow D^{*+} e^- \bar{\nu}$ candidates. The sideband used to subtract the combinatorial background is shown by long arrows and the signal region is indicated by short arrows. The data (histogram) are superimposed with the combinatorial background distribution (dashed curve).

Table 1

Yield of the $\bar{B}^0 \rightarrow D^{*+} e^- \bar{\nu}$ and the estimated background contributions. The errors are statistical only.

Raw Yield	1006 ± 32
Combinatorial background	100 ± 7
Correlated background	91 ± 10
Uncorrelated background	15 ± 4
Fake electron background	2 ± 2
Continuum background	32 ± 6
Final Yield	766 ± 35

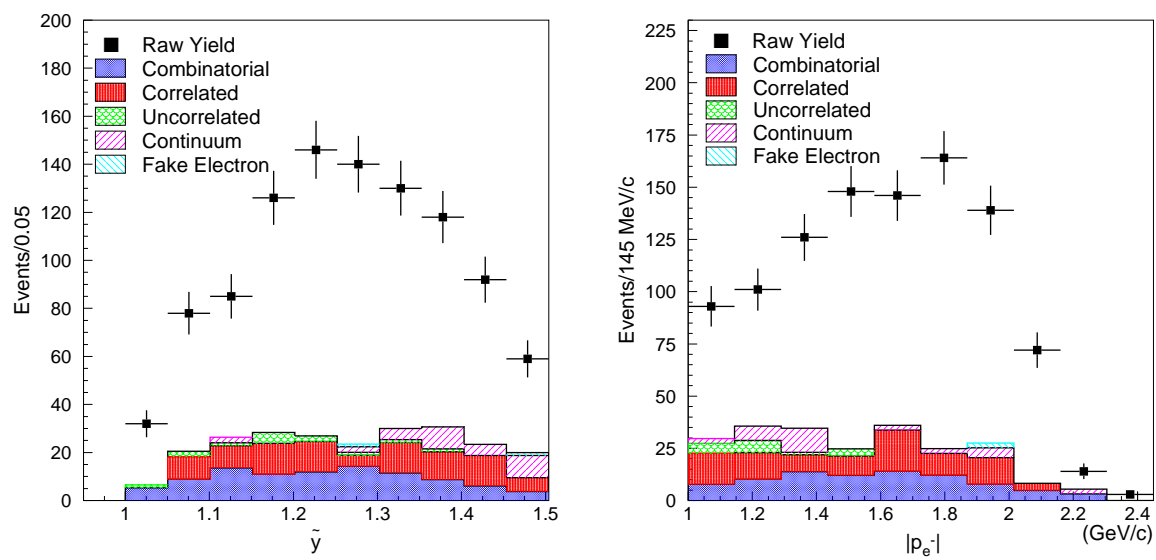


Fig. 2. Left (right) plot shows the raw yield and background as a function of \tilde{y} (electron momentum in the CM frame). From the bottom, combinatorial, correlated, uncorrelated, continuum and fake electron backgrounds are shown.

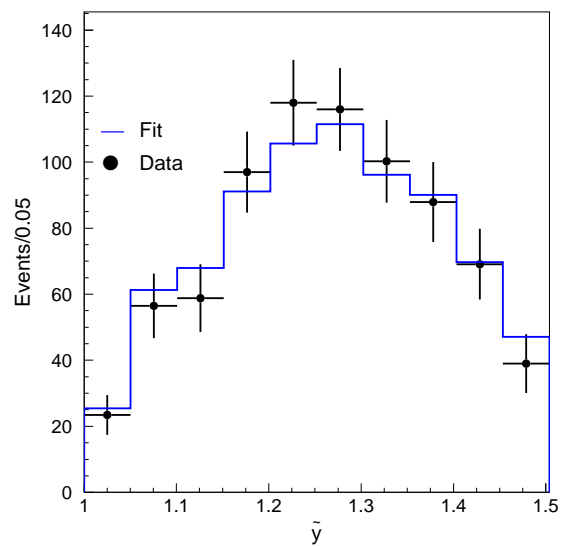


Fig. 3. Yield of $\bar{B}^0 \rightarrow D^{*+} e^- \bar{\nu}$ as a function of \tilde{y} . The points are background subtracted data and the histogram represents the fit to data.

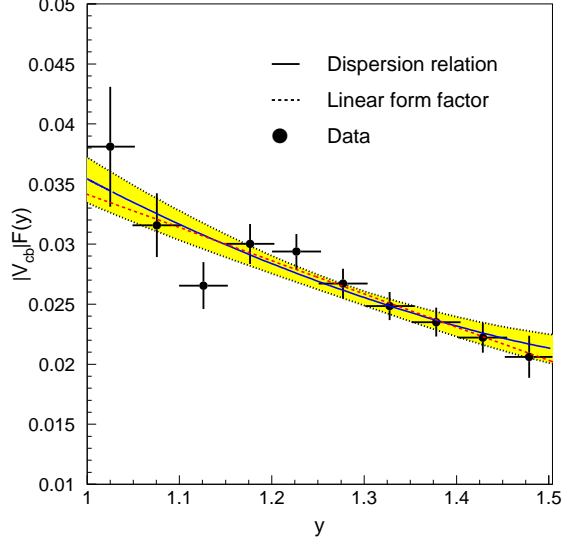


Fig. 4. $|V_{cb}|F(y)$ as a function of y . The data points with errors are derived from unfolding. The curves show the result obtained using the Caprini *et al.* form factor constrained by a dispersion relation (solid) and a linear form factor (dashed). The statistical uncertainty of the Caprini *et al.* form factor fit is shown by the shaded band.

Table 2

Summary of fit results according to different form factor (FF) parameterizations, where the errors are statistical only. Our main analysis uses values of $R_1(1)$, $R_2(1)$ from QCD sum rules.

FF shape & $R_1(1), R_2(1)$	$ V_{cb} F(1) \cdot 10^2$	$\rho_{A_1}^2$	ρ_F^2	$\mathcal{B}(\bar{B}^0 \rightarrow D^{*+}e^-\bar{\nu})$	χ^2/ndf
Dispersive & QCD sum rules	3.54 ± 0.19	1.35 ± 0.17	.	$(4.59 \pm 0.23)\%$	3.38/8
Dispersive & CLEO value	3.58 ± 0.19	1.45 ± 0.16	.	$(4.60 \pm 0.23)\%$	3.79/8
Linear & Heavy quark limit	3.42 ± 0.17	.	0.81 ± 0.12	$(4.57 \pm 0.24)\%$	2.23/8

Table 3

Summary of systematic errors. For each possible source the error on each of the three measured values is given.

Error Sources	$ V_{cb} F(1)$ (%)	$\rho_{A_1}^2$ (%)	$\mathcal{B}(\bar{B}^0 \rightarrow D^{*+}e^-\bar{\nu})$ (%)
$N_{B\bar{B}}$	0.5	.	1.0
$\tau_{\bar{B}^0}$	1.0	.	.
$\mathcal{B}(D^{*+} \rightarrow D^0\pi^+)$	0.4	.	0.7
$\mathcal{B}(D^0 \rightarrow K^-\pi^+)$	1.2	.	2.3
Tracking efficiency	2.5	.	5.1
Electron ID efficiency	1.0	.	1.9
D^0 reconstruction efficiency	1.4	.	2.8
Slow pion efficiency	2.6	1.2	5.0
Subtotal	4.3	1.2	8.3
y resolution	1.1	2.8	0.5
Combinatorial BG	1.0	0.1	1.9
Correlated BG (D^{**})	1.4	4.0	0.5
Uncorrelated BG	0.4	0.5	0.5
Fake electron BG	.	0.2	0.1
Continuum BG	0.5	2.9	0.9
MC statistics	1.7	4.4	1.3
$R_1(1), R_2(1)$	1.1	11.8	0.3
Subtotal	2.9	13.7	2.6
Total	5.2	13.8	8.7